



# 13

## Spectroscopic techniques: II Structure and interactions

A. HOFMANN

- 13.1 Introduction
- 13.2 Infrared and Raman spectroscopy
- 13.3 Surface plasmon resonance
- 13.4 Electron paramagnetic resonance
- 13.5 Nuclear magnetic resonance
- 13.6 X-ray diffraction
- 13.7 Small-angle scattering
- 13.8 Suggestions for further reading

### 13.1 INTRODUCTION

---

The overarching theme of techniques such as mass spectrometry (Chapter 9), electron microscopy and imaging (Chapter 4), analytical centrifugation (Chapter 3) and molecular exclusion chromatography (Chapter 11) is the aim to obtain clues about the structure of biomolecules and larger assemblies thereof. The spectroscopic techniques discussed in Chapters 12 and 13 are further complementary methods, and by assembling the jigsaw of pieces of information, one can gain a comprehensive picture of the structure of the biological object under study. In addition, the spectroscopic principles established in Chapter 12 are often employed as read-out in a huge variety of biochemical assays, and several more sophisticated technologies employ these basic principles in a 'hidden' way.

In the previous chapter, we established that the electromagnetic spectrum is a continuum of frequencies from the long wavelength region of the radio frequencies to the high-energy  $\gamma$ -rays of nuclear origin. While the methods and techniques discussed in Chapter 12 concentrated on the use of visible and UV light, there are other spectroscopic techniques that employ electromagnetic radiation of higher as well as lower energy. Another shared property of the techniques in this chapter is the higher level of complexity in undertaking. These applications are usually employed at a later stage of biochemical characterisation and aimed more at investigation of the three-dimensional structure, and in the case of proteins and peptides, address the tertiary and quaternary structure.

## 13.2 INFRARED AND RAMAN SPECTROSCOPY

### 13.2.1 Principles

Within the electromagnetic spectrum (Fig. 12.1), the energy range below the UV/Vis is the infrared region, encompassing the wavelength range of about 700 nm to 25  $\mu\text{m}$ , and thus reaching from the red end of the visible to the microwave region. The absorption of infrared light by a molecule results in transition to higher levels of **vibration** (Fig. 12.3).

For the purpose of this discussion, the bonds between atoms can be considered as flexible springs, illustrating the constant vibrational motion within a molecule (Fig. 13.1). Bond vibrations can thus be either **stretching** or **bending** (deformation) actions. Theory predicts that a molecule with  $n$  atoms will have a total of  $3n - 6$  fundamental vibrations ( $3n - 5$ , if the molecule is linear):  $2n - 5$  bending, and  $n - 1$  stretching modes (Fig. 13.2).

Infrared and Raman spectroscopy give similar information about a molecule, but the criteria for the phenomena to occur are different for each type. For asymmetric molecules, incident infrared light will give rise to an absorption band in the infrared spectrum, as well as a peak in the Raman spectrum. However, as shown in Fig. 13.2, symmetric molecules, such as for example  $\text{CO}_2$ , that possess a centre of symmetry show a selective behaviour: bands that appear in the infrared spectrum do not appear in the Raman spectrum, and vice versa.

An **infrared spectrum** arises from the fact that a molecule absorbs incident light of a certain wavelength which will then be 'missing' from the transmitted light. The recorded spectrum will show an absorption band.

A **Raman spectrum** arises from the analysis of scattered light, and we have already introduced the basics of inelastic light scattering in Section 12.6.3. The largest part of an incident light beam passes through the sample (transmission). A small part is scattered isotropically, i.e. uniformly in all directions (**Rayleigh scatter**), and possesses the same wavelength as the incident beam. The Raman spectrum arises from the fact

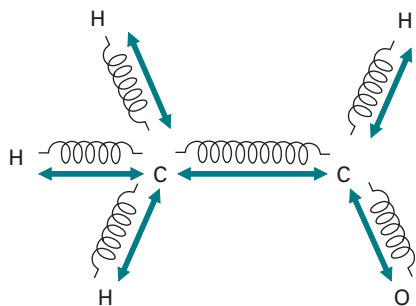


Fig. 13.1 Possible stretching vibrations in acetaldehyde.



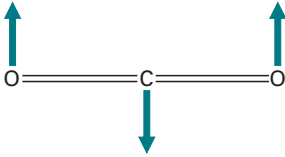
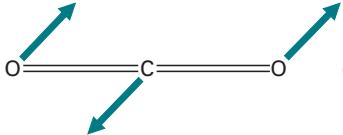
Mode		Wavenumber	IR	Raman
Stretching, symmetric	 $\text{O}=\text{C}=\text{O}$	$1340\text{ cm}^{-1}$	–	+
Stretching, asymmetric	 $\text{O}=\text{C}=\text{O}$	$2349\text{ cm}^{-1}$	+	–
Deformation	 $\text{O}=\text{C}=\text{O}$	$667\text{ cm}^{-1}$	+	–
Deformation	 $\text{O}=\text{C}=\text{O}$	$667\text{ cm}^{-1}$	+	–

Fig. 13.2 Normal vibrational modes for  $\text{CO}_2$ . For symmetric molecules that possess a centre of symmetry, bands that appear in the IR do not appear in the Raman spectrum.

that a very small proportion of light scattered by the sample will have a different frequency than the incident light. As different vibrational states are excited, energy portions will be missing, thus giving rise to peaks at lower frequencies than the incident light (**Stokes lines**). Notably, higher frequencies are also observed (**anti-Stokes lines**); these arise from excited molecules returning to ground state. The emitted energy is dumped onto the incident light which results in scattered light of higher energy than the incident light.

The criterion for a band to appear in the infrared spectrum is that the transition to the excited state is accompanied by a change in **dipole moment**, i.e. a change in charge displacement. Conversely, the criterion for a peak to appear in the Raman spectrum is a change in **polarisability** of the molecule during the transition.

### Infrared spectroscopy

The fundamental frequencies observed are characteristic of the **functional groups** concerned, hence the term **fingerprint**. Figure 13.3 shows the major bands of an FT-IR spectrum of the drug phenacetin. As the number of functional groups increases in more complex molecules, the absorption bands become more difficult to assign. However, groups of certain bands regularly appear near the same wavelength and may be assigned to specific functional groups. Such group frequencies are thus extremely helpful in structural diagnosis. A more detailed analysis of the structure of a molecule is possible, because the wavenumber associated with a particular functional group varies slightly, owing to the influence of the molecular environment.

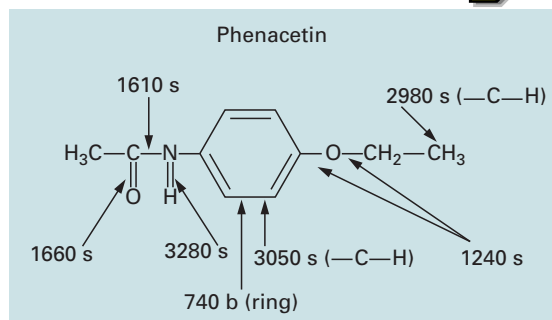
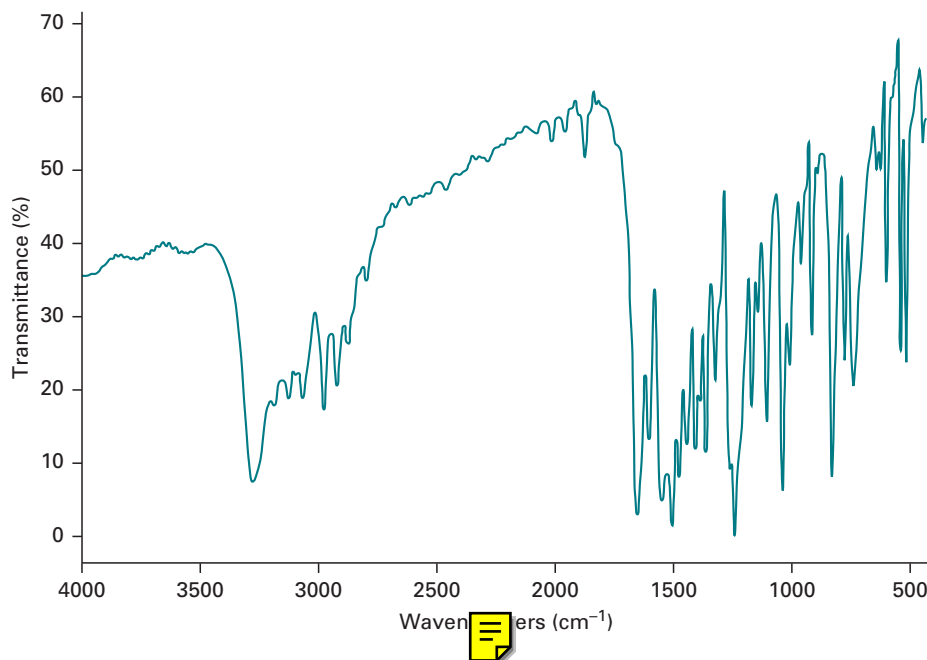


Fig. 13.3 FT-IR spectrum of phenacetin, the historically first synthetic fever reducer to go on the market. Bands at the appropriate wavenumbers ( $\text{cm}^{-1}$ ) are shown, indicating the bonds with which they are associated, and the type (s, stretching; b, bending).

For example, it is possible to distinguish between C-H vibrations in methylene ( $-\text{CH}_2-$ ) and methyl groups ( $-\text{CH}_3$ ).

### Raman spectroscopy

The assignment of peaks in Raman spectra usually requires consideration of peak position, intensity and form, as well as **depolarisation**. This allows identification of the type of **symmetry of individual vibrations**, but not the determination of structural elements of a molecule. The depolarisation is calculated as the ratio of two intensities with perpendicular and parallel polarisation with respect to the incident beam. The use of lasers as light source for Raman spectroscopy easily facilitates the use of linearly polarised light. Practically, the Raman spectrum is measured twice. In the second measurement, the polarisation plane of the incident beam is rotated by  $90^\circ$ .

### 13.2.2 Instrumentation

The most common source for infrared light is white-glowing zircon oxide or the so-called globar made of silicon carbide with a glowing temperature of 1500 K. The beam of infrared light passes a monochromator and splits into two separate beams: one runs through the sample, the other through a reference made of the substance the sample is prepared in. After passing through a splitter alternating between both beams, they are reflected into the detector. The reference is used to compensate for fluctuations in the source, as well as to cancel possible effects of the solvent. Samples of solids are either prepared in thick suspensions (mulls) such as nujol, and held as layers between NaCl planes or pressed into KBr disks. Non-covalent materials must be used for sample containment and in the optics, as these materials are transparent to infrared. All materials need to be free of water, because of the strong absorption of the O–H vibration.

Analysis using a Michelson interferometer enables **Fourier transform infrared spectroscopy** (FT-IR). The entire light emitted from the source is passed through the sample at once, and then split into two beams that are reflected back onto the point of split (interferometer plate). Using a movable mirror, path length differences are generated between both beams yielding an interferogram that is recorded by the detector. The interferogram is related with a conventional infrared spectrum by a mathematical operation called Fourier transform (see also Fig. 13.9).

For Raman spectroscopy, aqueous solutions are frequently used, since water possesses a rather featureless weak Raman spectrum. The Raman effect can principally be observed with bright, monochromatic light of any wavelength; however, light between the visible region of the spectrum is normally used due to few unwanted absorption effects. The ideal light source for Raman spectrometers is therefore a laser. Because the Raman effect is observed in light scattered off the sample, typical spectrometers use a 90° configuration.

### 13.2.3 Applications

The use of infrared and Raman spectroscopy is mainly in chemical and biochemical research of small compounds such as drugs, metabolic intermediates and substrates. Examples are the identification of synthesised compounds, or identification of sample constituents (e.g. in food) when coupled to a separating method such as gas chromatography (GC-IR).

FT-IR is increasingly used for analysis of peptides and proteins. The peptide bond gives rise to nine characteristic bands, named amide A, B, I, II, III, . . . , VII. The amide I ( $1600\text{--}1700\text{ cm}^{-1}$ ) and amide II ( $1500\text{--}1600\text{ cm}^{-1}$ ) bands are the major contributors to the protein infrared spectrum. Both bands are directly related to the backbone conformation and have thus been used for assessment of the secondary structure of peptides and proteins. The interpretation of spectra of molecules with a large number of atoms usually involves deconvolution of individual bands and second derivative spectra.

**Time-resolved FT-IR** (trFT-IR) enables the observation of protein reactions at the sub-millisecond timescale. This technique has been established by investigation of

the light-driven proton pump bacteriorhodopsin. For instance, the catalytic steps in the proton pumping mechanism have been validated with trFT-IR, and involve transfer of a proton from the Schiff base ( $R_1R_2C=N-R_3$ ) to a catalytic aspartate residue, followed by re-protonation of a second catalytic aspartate residue.

## 13.3 SURFACE PLASMON RESONANCE

### 13.3.1 Principles

**Surface plasmon resonance** (SPR) is a surface-sensitive method for monitoring smallest changes of the **refractive index** or the thickness of thin films. It is mainly used for monitoring the interaction of two components (e.g. ligand and receptor, Section 17.3.2) one of which is immobilised on a **sensor chip** surface (Fig. 13.4a), such as a hydrogel layer on a glass slide, via either biotin-avidin interactions or covalent coupling using amine or thiol reagents similar to those used for cross-linking to affinity chromatography resins (see Section 11.8). Typical surface concentrations of the bound protein component are in the range of  $1\text{--}5\text{ ng mm}^{-2}$ . The sensor chip forms one wall of a microflow cell so that an aqueous solution of the ligand can be pumped at a continuous, pulse-free rate across the surface. This ensures that the concentration of ligand at the surface is maintained at a constant value. Environmental parameters such as temperature, pH and ionic strength are carefully controlled, as is the duration of exposure of the immobilised component to the ligand. Replacing the ligand solution by a buffer solution enables investigation of the dissociation of bound ligand.

Binding of ligand to the immobilised component causes an increase in mass at the surface of the chip. Vice versa, dissociation of ligand causes a reduction of mass. These mass changes, in turn, affect the refractive index of the medium at the surface of the chip, the value of which determines the propagation velocity of electromagnetic radiation in that medium.

**Plasmon** is a term for a collection of conduction electrons in a metal or semiconductor. Excitation of a plasmon wave requires an optical prism with a metal film of about 50 nm thickness. **Total internal reflection** (TIR) occurs when a light beam travelling through a medium of higher refractive index (e.g. glass prism with gold-coated surface) meets at an interface with a medium of lower refractive index (e.g. aqueous sample) at an angle larger than the critical angle. TIR of an incident light beam at the prism-metal interface elicits a propagating plasmon wave by leaking an electrical field intensity, called an **evanescent field wave**, into the medium of lower refractive index where it decays at an exponential rate and effectively only travels one wavelength.

Since the interface between the prism and the medium is coated with a thin layer of gold, incident photons excite a vibrational state of the electrons of the conducting band of the metal. In thin metal films this propagates as a longitudinal vibration. The electrons vibrate with a resonance frequency (hence the term ‘resonance’) that is dependent on metal and prism properties, as well as the wavelength and the angle of

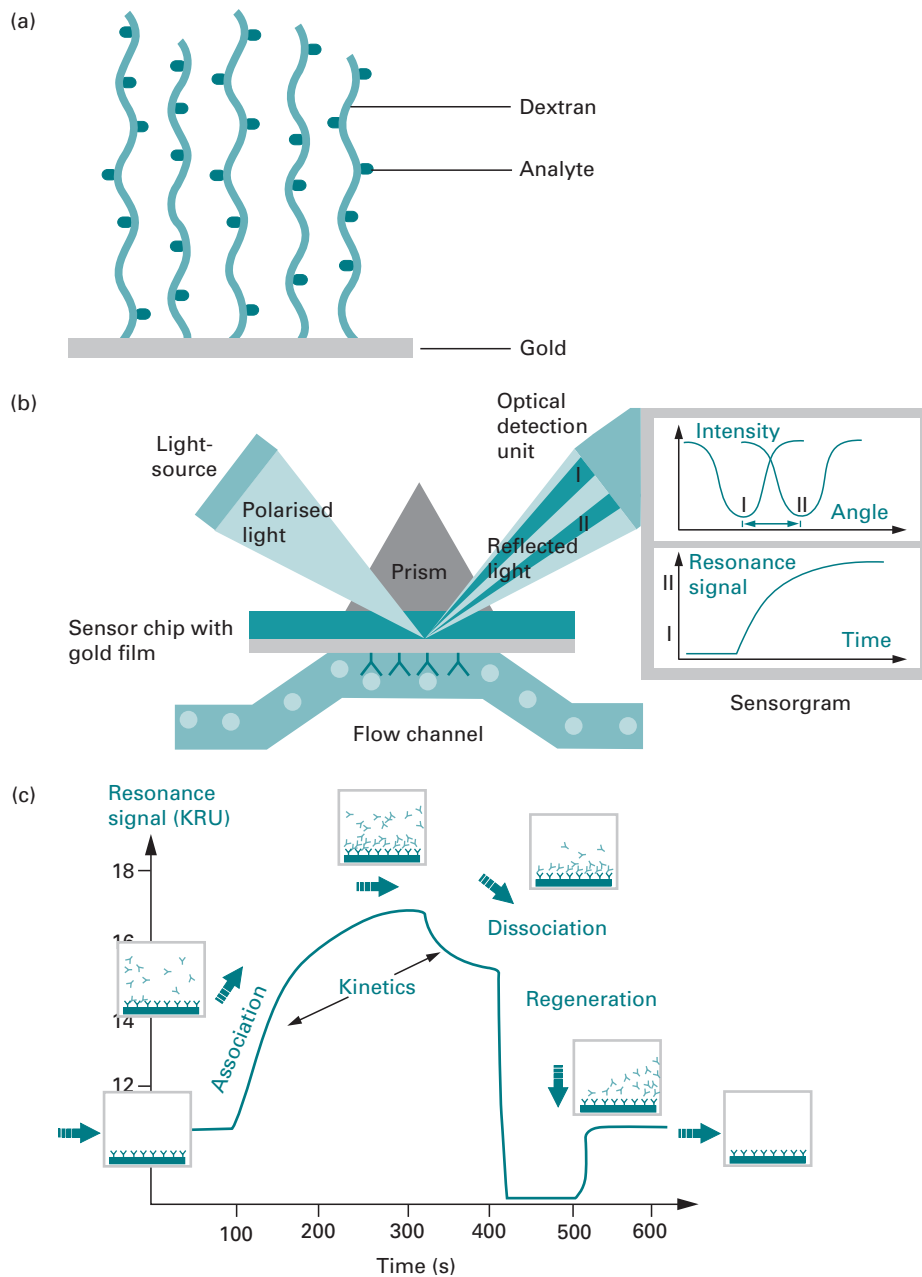


Fig. 13.4 The principles of surface plasmon resonance technology. (a) The sensor 'chip' surface. (b) The flow channel. Insert: change in intensity of reflected light as a function of angle of incidence of the light beam, and change in resonance signal as a function of time. (c) The sensorgram. (Reproduced by permission of GE Healthcare.)

the incident beam. Excitation of the plasmon wave leads to a decreased intensity of the **reflected light**. Thus, SPR produces a dip in the reflected light intensity at a specific angle of reflection. The propagating surface plasmon wave enhances the amplitude of the evanescent field wave, which extends into the sample region (Fig. 13.4b).

When binding to the chip occurs, the refractive index on the sample side of the interface increases. This alters the angle of incidence required to produce the SPR effect and hence also alters the angle of reflected light. The change in angle brings about a change in detector position, which can be plotted against time to give a sensorgram reading (Fig. 13.4c). The angle is expressed in resonance units (RU), such that 1000 RU corresponds to a change in mass at the surface of the chip of about  $1 \text{ ng mm}^{-2}$ .

Since in SPR instruments the angle and the wavelength of the incident beam are constant, a shift in the plasmon resonance leads to a change in the intensity of the reflected beam. The shift is restricted locally and happens only in areas where the optical properties have changed. The usage of an array detector as compared to a single detector cell therefore allows for measurement of an SPR image. SPR can detect changes in the refractive index of less than  $10^{-4}$  or changes in layer heights of about 1 nm. This enables not only the detection of binding events between biomolecules but also binding at protein domains or changes in molecular monolayers with a lateral resolution of a few  $\mu\text{m}$ . For SPR, light of wavelengths between infrared (IR) and near-infrared (NIR) may be used. In general, the higher the wavelength of the light used the better the sensitivity but the less the lateral resolution. Vice versa, if high lateral resolution is required, red light is to be used because the propagation length of the plasmon wave is approximately proportional to the wavelength of the exciting light.

### 13.3.2 Applications

The SPR technique enjoys frequent use in modern life science laboratories, due to its general applicability and the fact that there are no special requirements for the molecules to be studied (**label-free**), such as fluorescent properties, spectral labels or radio labels. It can even be used with coloured or opaque solutions.

Generally, all two-component binding reactions can be investigated, which opens a variety of applications in the areas of drug design (protein–ligand interactions), as well as mechanisms of membrane-associated proteins (protein–membrane binding) and DNA-binding proteins. SPR has thus successfully been used to study the kinetics of receptor–ligand interactions, antibody–antigen and protein–protein interactions. The method is extensively used in proteomic research and drug development.

#### SPR imaging

The focus of SPR imaging experiments has shifted in recent years from characterisation of ultrathin films to analysis of biosensor chips, especially affinity sensor arrays. SPR imaging can detect DNA–DNA, DNA–protein and protein–protein interactions in a two-dimensional manner. The detection limit for such biosensor chips is in the order of nM to fM. Apart from the detection of binding events as such, the quality of binding (low affinity, high affinity) can also be assessed by SPR imaging. Promising future applications for SPR imaging include peptide arrays that can be prepared on modified gold surfaces. This can prove useful for assessing peptide–antibody interactions. The current time resolution of less than 1 s for an entire image also allows for high-throughput screenings and *in situ* measurements.



## 13.4 ELECTRON PARAMAGNETIC RESONANCE

Prior to any detailed discussion of electron paramagnetic resonance (EPR) and nuclear magnetic resonance (NMR) methods, it is worthwhile considering the more general phenomena applicable to both.

### 13.4.1 Magnetic phenomena

Magnetism arises from the **motion of charged particles**. This motion is controlled by internal forces in a system. For the purpose of this discussion, the major contribution to magnetism in molecules is due to the **spin** of the charged particle.

In chemical bonds of a molecule, the negatively charged electrons have a spin controlled by strict **quantum rules**. A bond is constituted by two electrons with opposite spins occupying the appropriate molecular orbital. According to the **Pauli principle**, the two electrons must have opposite spins, leading to the term **paired electrons**. Each of the spinning electronic charges generates a magnetic effect, but in electron pairs the effect is almost self-cancelling. In atoms, a value for magnetic susceptibility may be calculated and is of the order of  $-10^{-6} \text{ g}^{-1}$ . This **diamagnetism** is a property of all substances, because they all contain the minuscule magnets, i.e. electrons. Diamagnetism is temperature independent.

If an electron is unpaired, there is no counterbalancing opposing spin and the magnetic susceptibility is of the order of  $+10^{-3}$  to  $+10^{-4} \text{ g}^{-1}$ . The effect of an **unpaired electron** exceeds the 'background' diamagnetism, and gives rise to **paramagnetism**. Free electrons can arise in numerous cases. The most notable example is certainly the paramagnetism of metals such as iron, cobalt and nickel, which are the materials that permanent magnets are made of. The paramagnetism of these metals is called **ferromagnetism**. In biochemical investigations, systems with free electrons (radicals) are frequently used as probes.

Similar arguments can be made regarding **atomic nuclei**. The nucleus of an atom is constituted by protons and neutrons, and has a net charge that is normally compensated by the extra-nuclear electrons. The number of all nucleons ( $Z$ ) is the sum of the number of protons ( $P$ ) and the number of neutrons ( $N$ ).  $P$  and  $Z$  determine whether a nucleus will exhibit paramagnetism. Carbon-12 ( $^{12}\text{C}$ ), for example, consists of six protons ( $P = 6$ ) and six neutrons ( $N = 6$ ) and thus has  $Z = 12$ .  $P$  and  $Z$  are even, and therefore the  $^{12}\text{C}$  nucleus possesses no nuclear magnetism. Another example of a nucleus with no residual magnetism is oxygen-16 ( $^{16}\text{O}$ ). All other nuclei with  $P$  and  $Z$  being uneven possess residual nuclear magnetism.

The way in which a substance behaves in an externally applied magnetic field allows us to distinguish between dia- and paramagnetism. A paramagnetic material is attracted by an external magnetic field, while a diamagnetic substance is rejected. This principle is employed by the **Guoy balance**, which allows quantification of magnetic effects. A balance pan is suspended between the poles of a suitable electro-magnet supplying the external field. The substance under test is weighed in air with the current switched off. The same sample is then weighed again with the current

(i.e. external magnetic field) on. A paramagnetic substance appears to weigh more, and a diamagnetic substance appears to weigh less.

### 13.4.2 The resonance condition

In both EPR and NMR techniques, two possible energy states exist for either electronic or nuclear magnetism in the presence of an **external magnetic field**. In the low-energy state, the field generated by the spinning charged particle is parallel to the external field. Conversely, in the high-energy state, the field generated by the spinning charged particle is antiparallel to the external field. When enough energy is input into the system to cause a transition from the low- to the high-energy state, the condition of resonance is satisfied. Energy must be absorbed as a discrete dose (quantum)  $h\nu$ , where  $h$  is the Planck constant and  $\nu$  is the frequency (see equation 12.1). The quantum energy required to fulfil the resonance condition and thus enable transition between the low- and high-energy states may be quantified as:

$$h\nu = g\beta B \quad (13.1)$$



where  $g$  is a constant called **spectroscopic splitting factor**,  $\beta$  is the magnetic moment of the electron (termed the Bohr magneton), and  $B$  is the strength of the applied external magnetic field. The frequency  $\nu$  of the absorbed radiation is a function of the paramagnetic species  $\beta$  and the applied magnetic field  $B$ . Thus, either  $\nu$  or  $B$  may be varied to the same effect.

With appropriate external magnetic fields, the frequency of applied radiation for EPR is in the microwave region, and for NMR in the region of radio frequencies. In both techniques, two possibilities exist for determining the absorption of electromagnetic energy (i.e. enabling the resonance phenomenon):

- constant frequency  $\nu$  is applied and the external magnetic field  $B$  is swept; or
- constant external magnetic field  $B$  is applied and the appropriate frequency  $\nu$  is selected by sweeping through the spectrum.

For technical reasons, the more commonly used option is a sweep of the external magnetic field.

### 13.4.3 Principles

The absorption of energy is recorded in the EPR spectrum as a function of the magnetic induction measured in  (T) which is proportional to the **magnetic field strength** applied. The area under  absorption peak is proportional to the number of unpaired electron spins. Most commonly, the first derivative of the absorption peak is the signal that is actually recorded.

For a delocalised electron, as observed e.g. in free radicals, the  $g$  value is 2.0023; but for localised electrons such as in transition metal atoms,  $g$  varies, and its precise value contains information about the nature of bonding in the environment of the unpaired electron within the molecule. When resonance occurs, the absorption

peak is broadened owing to interactions of the unpaired electron with the rest of the molecule (**spin–lattice interactions**). This allows further conclusions as to the molecular structure.

High-resolution EPR may be performed by examining the **hyperfine splitting** of the absorption peak which is caused by interaction of the unpaired electron with adjacent nuclei, thus yielding information about the spatial location of atoms in the molecule. The proton hyperfine splitting for free radicals occurs in the range of  $0\text{--}3 \times 10^{-3}$  T, and yields data analogous to those obtained in high-resolution NMR (see Section 13.5).

The effective resolution of an EPR spectrum can be considerably improved by combining the method with NMR, a technique called **electron nuclear double resonance** (ENDOR). Here, the sample is irradiated simultaneously with microwaves for EPR and radio frequencies (RF) for NMR. The RF signal is swept for fixed points in the EPR spectrum, yielding the EPR signal height versus nuclear RF. This approach is particularly useful when there are a large number of nuclear levels that broaden the normal electron resonance lines.

The technique of **electron double resonance** (ELDOR) finds an application in the separation of overlapping multiradical spectra and the study of relaxation phenomena, for example chemical spin exchange. In ELDOR, the sample is irradiated with two microwave frequencies simultaneously. One is used for observation of the EPR signal at a fixed point in the spectrum, the other is used to sweep other parts of the spectrum. The recorded spectrum is plotted as a function of the EPR signal as a function of the difference of the two microwave frequencies.

#### 13.4.4 Instrumentation

Figure 13.5 shows the main components of an EPR instrument. The magnetic fields generated by the electromagnets are of the order of 50 to 500 mT, and variations of less than  $10^{-6}$  are required for highest accuracy. The monochromatic microwave radiation is produced in a **klystron** oscillator with wavelengths around 3 cm (9 GHz).

The samples are required to be in the solid state; hence biological samples are usually frozen in liquid nitrogen. The technique is also ideal for investigation of membranes and membrane proteins. Instead of plotting the absorption  $A$  versus  $B$ , it is the first-order differential ( $dA/dB$ ) that is usually plotted against  $B$  (Fig. 13.6). Such a shape is called a ‘line’ in EPR spectroscopy. Generally, there are relatively few unpaired electrons in a molecule, resulting in fewer than 10 lines, which are not closely spaced.

#### 13.4.5 Applications

##### Metalloproteins

EPR spectroscopy is one of the main methods to study metalloproteins, particularly those containing molybdenum (xanthine oxidase), copper (cytochrome oxidase, copper blue enzymes) and iron (cytochrome, ferredoxin). Both copper and non-haem iron, which do not absorb in the UV/Vis region, possess EPR absorption peaks in one

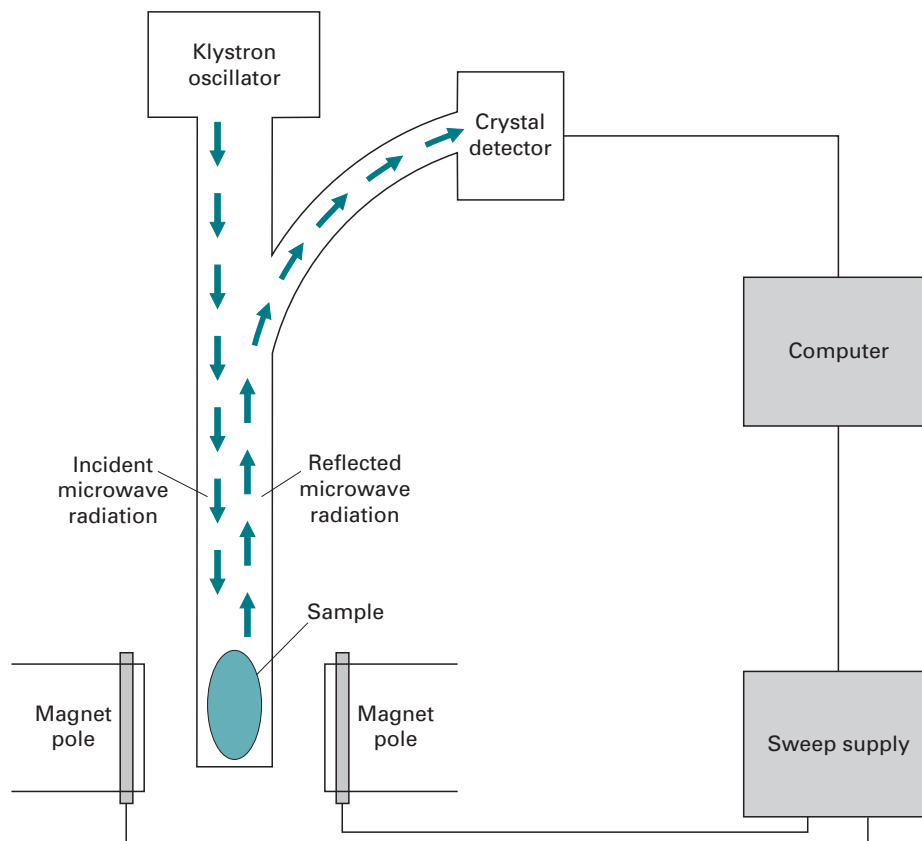


Fig. 13.5 Diagram of an EPR spectrometer.

of their oxidised states. The appearance and disappearance of their EPR signals are used to monitor the activity of these proteins in the multi-enzyme systems of intact mitochondria and chloroplasts, as well as in isolated enzymes. In many metallo-proteins, the ligands coordinating the metal ion are the amino acid residues of the protein. Coordination chemistry requires a specific stereochemical structure of the ligands, and EPR studies show that the geometry is frequently distorted in proteins when compared to model systems. Such distortions may be related to biological function.

### Spin labels

Spin labels are stable and non-reactive unpaired electrons used as reporter groups or probes for EPR. The procedure of spin labelling is the attachment of these probes to biological molecules that lack unpaired electrons. The label can be attached to either a substrate or a ligand. Often, a spin label contains the nitric oxide moiety. These labels enable the study of events that occur with a frequency of  $10^7$  to  $10^{11} \text{ s}^{-1}$ . If the motion is restricted in some directions, only anisotropic motion (movement in one particular direction) may be studied, for example in membrane-rigid spin labels in bilayers. Here, the label is attached so that the NO group lies parallel to the long axis of the lipid.

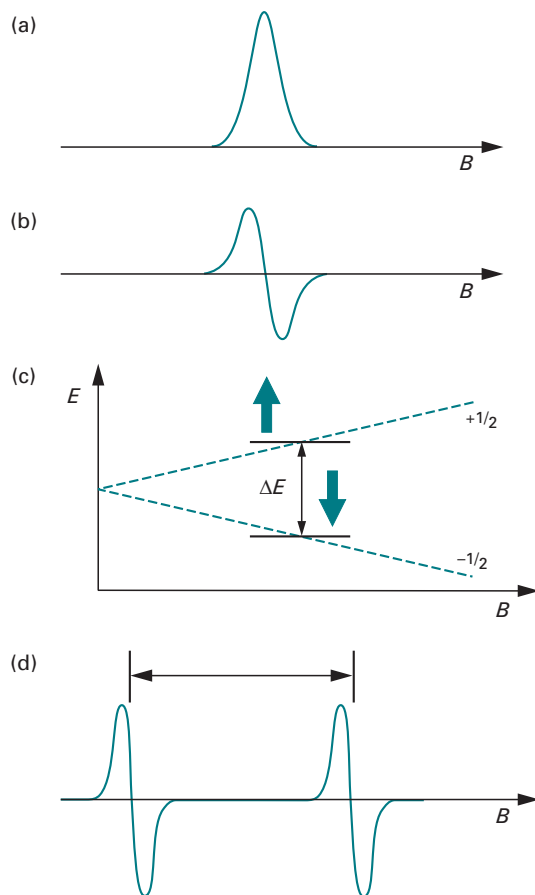


Fig. 13.6 Instead of the absorption signal (a), EPR spectrometry records its first derivative (b). (c) The energy of the two spin states of a free electron is shown as a function of the external magnetic field  $B$ . Resonance happens when the energy of the applied microwave radiation is the same as the energy difference  $\Delta E$ . (d) Hyperfine splitting due to coupling of an unpaired electron with a nuclear spin of  $1/2$ . For the hydrogen atom, the distance between the two signals is 50.7 mT.

Intramolecular motions and lateral diffusion of lipid through the membrane, as well as the effect of proteins and other factors on these parameters may be observed. Quantification of effects often involves calculation of the **order parameter**  $Z$ . Spin-labelled lipids are either concentrated into one region of the bilayer or randomly incorporated into model membranes. The diffusion of spin labels allows them to come into contact with each other, which causes line-broadening in the spectrum. Labelling of phospholipids with 2,2,6,6-tetramethylpiperidine-1-oxyl (TEMPO) is used for measurement of the flip rate of phospholipids between inner and outer surfaces as well as lateral diffusion.

### Free radicals

Molecules in their **triplet states** (Fig. 12.8) have unpaired electrons and thus are amenable to EPR spectroscopy. Such molecules possess the property of phosphorescence

and EPR may deliver data complementary to the UV/Vis region of the spectrum. For instance, free radicals due to the triplet state of tryptophan have been observed in cataractuous lenses.

Spin trapping is a process whereby an unstable free radical is being stabilised by reaction with a compound such as 5,5-dimethylpyrroline-1-oxide (DMPO). Hyperfine splittings (Fig. 13.6) are observed that depend upon the nature of the radical.

Carcinogenesis is an area where free radicals have been implicated. While free radicals promote the generation of tumours through damage due to their high reactivity, there is, in general, a lower concentration of radicals in tumours than in normal tissue. Also, a gradient has been observed with higher concentrations of radicals in the peripheral non-necrotic surface layers than in the inner regions of the tumour. EPR has been used to study implanted tumours in mice, but also in evaluation of potential chemical carcinogens. Polycyclic hydrocarbons, such as naphthalene, anthracene and phenanthrene, consist of multiple aromatic ring systems. These extended aromatic systems allow for single free electrons to be accommodated and thus yield long-lived free radicals, extending the periods of time in which damage can be done. Many of the precursors of these radicals exist in natural sources such as coal tar, tobacco smoke and other products of combustion, hence the environmental risk. Another source of free radicals is irradiation with UV light or  $\gamma$ -rays. Ozone is an oxygen radical that is

#### Example 1 **FREE RADICALS IN THE HEALTHY ORGANISM**

An important concern for humans today is environmental pollution and its effects on our bodies. Environmental pollutants – from auto exhaust, second-hand cigarette smoke, pesticides, or even ultraviolet radiation from the Sun – create what are known as free radicals in our bodies.

A lot of metabolic studies have made use of EPR spectroscopy. Free radicals are found in many metabolic pathways and as degradation products of drugs and toxins. Electron transfer mechanisms in mitochondria and chloroplasts involve paramagnetic species, such as the Fe-S centres. Other RedOx processes involving the flavin derivatives FAD, FMN and semiquinons lend themselves readily to exploration by EPR spectroscopy. The signal of  $g = 2.003$  mainly stems from mitochondria. However, different cell lines show different intensities, because this phenomenon also depends on the metabolic state. Factors increasing the metabolic activity also lead to an increase in organic radical signal. Many studies in this context have focussed on the free radical polymer melanin (the skin pigment) and the ascorbyl radical (vitamin C metabolite).

Nitric oxide (NO) operates as a physiological messenger regulating the nervous, immune and cardiovascular systems. It has been implicated in septic (toxic) shock, hypertension, stroke and neurodegenerative diseases. Although NO is involved in normal synaptic transmission, excess levels are neurotoxic. Enzymes such as superoxide dismutase attenuate the neurotoxicity by removal of radical oxygen species, hence limiting their availability for reaction with NO to produce peroxynitrite.

present as a protective shield around the Earth, filtering the dangers of cosmic UV irradiation by complex radical chemistry. The pollution of the Earth's atmosphere with radical-forming chemicals has destroyed large parts of the ozone layer, increasing the risk of skin cancer from sun exposure. EPR can be used to study biological materials, including bone or teeth, and detect radicals formed due to exposure to high energy radiation.

Another major application for EPR is the examination of irradiated foodstuffs for residual free radicals, and it is mostly used to establish whether packed food has been irradiated.

## 13.5 NUCLEAR MAGNETIC RESONANCE

The essential background theory of the phenomena that allow NMR to occur have been introduced in Sections 13.4.1 and 13.4.2. However, the miniature magnets involved here are not electrons, but the nuclei. The specific principles, instrumentation and applications are discussed below.

### 13.5.1 Principles

Most studies in organic chemistry involve the use of  $^1\text{H}$ , but NMR spectroscopy with  $^{13}\text{C}$ ,  $^{15}\text{N}$  and  $^{31}\text{P}$  isotopes is frequently used in biochemical studies. The resonance condition in NMR is satisfied in an external magnetic field of several hundred mT, with absorptions occurring in the region of radio waves (frequency 40 MHz) for resonance of the  $^1\text{H}$  nucleus. The actual field scanned is small compared with the field strengths applied, and the radio frequencies absorbed are specifically stated on such spectra.

Similar to other spectroscopic techniques discussed earlier, the energy input in the form of electromagnetic radiation promotes the transition of 'entities' from lower to higher energy states (Fig. 13.7). In case of NMR, these entities are the nuclear magnetic spins which populate energy levels according to quantum chemical rules. After a certain time-span, the spins will return from the higher to the lower energy level, a process that is known as **relaxation**.

The energy released during the transition of a nuclear spin from the higher to the lower energy state can be emitted as heat into the environment and is called **spin-lattice relaxation**. This process happens with a rate of  $T_1^{-1}$ , and  $T_1$  is termed the **longitudinal relaxation time**, because of the change in magnetisation of the nuclei parallel to the field. The transverse magnetisation of the nuclei is also subject to change over time, due to interactions between different nuclei. The latter process is thus called **spin-spin relaxation** and is characterised by a **transverse relaxation time**  $T_2$ .

The molecular environment of a proton governs the value of the applied external field at which the nucleus resonates. This is recorded as the **chemical shift** ( $\delta$ ) and is measured relative to an internal standard, which in most cases is tetramethylsilane

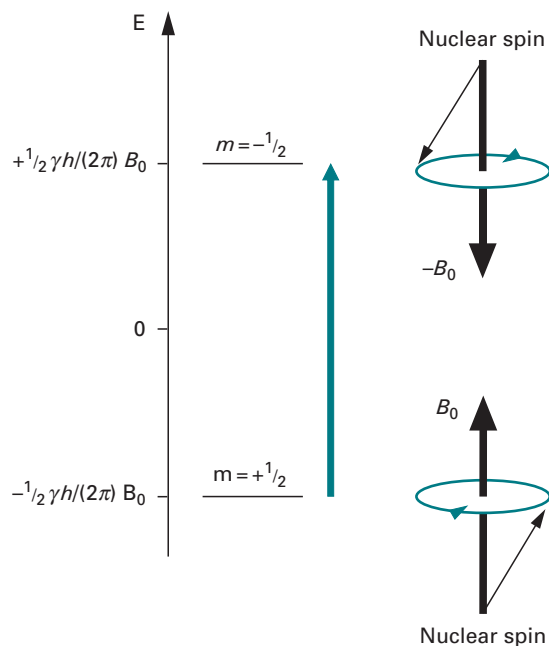


Fig. 13.7 Energy levels of a proton in the magnetic field  $B_0$ . The nuclear spin of a nucleus is characterised by its magnetic quantum number  $m$ . For protons,  $m$  can only adopt  $+\frac{1}{2}$  and  $-\frac{1}{2}$ . The corresponding energies are calculated by  $-m\gamma h/(2\pi)H_0$ , where  $\gamma$  is a constant characteristic for a particular nucleus,  $h$  is the Planck constant, and  $H_0$  is the strength of the magnetic field  $B_0$ .

(TMS;  $(\text{H}_3\text{C})_4\text{Si}$ ) because it contains 12 identical protons. The chemical shift arises from the applied field inducing secondary fields of about 0.15–0.2 mT at the proton by interacting with the adjacent bonding electrons.

- If the induced field opposes the applied field, the latter will have to be at a slightly higher value for resonance to occur. The nucleus is said to be **shielded**, the magnitude of the shielding being proportional to the electron-withdrawing power of proximal substituents.
- Alternatively, if the induced and applied fields are aligned, the latter is required to be at a lower value for resonance. The nucleus is then said to be **deshielded**.

Usually, **deuterated solvents** such as  $\text{CDCl}_3$  are used for sample preparation of organic compounds. For peptides and proteins  $\text{D}_2\text{O}$  is the solvent of choice. Because the stability of the magnetic field is critical for NMR spectroscopy, the magnetic flux needs to be tuned, e.g. by locking with deuterium resonance frequencies. The use of deuterated solvents thus eliminates the need for further experiments.

The chemical shift is plotted along the  $x$ -axis, and measured in p.p.m. instead of the actual magnetic field strengths. This conversion makes the recorded spectrum independent of the magnetic field used. The signal of the internal standard TMS appears at  $\delta = 0$  p.p.m. The type of proton giving rise to a particular band may thus be identified by the resonance peak position, i.e. its chemical shift, and the area under each peak



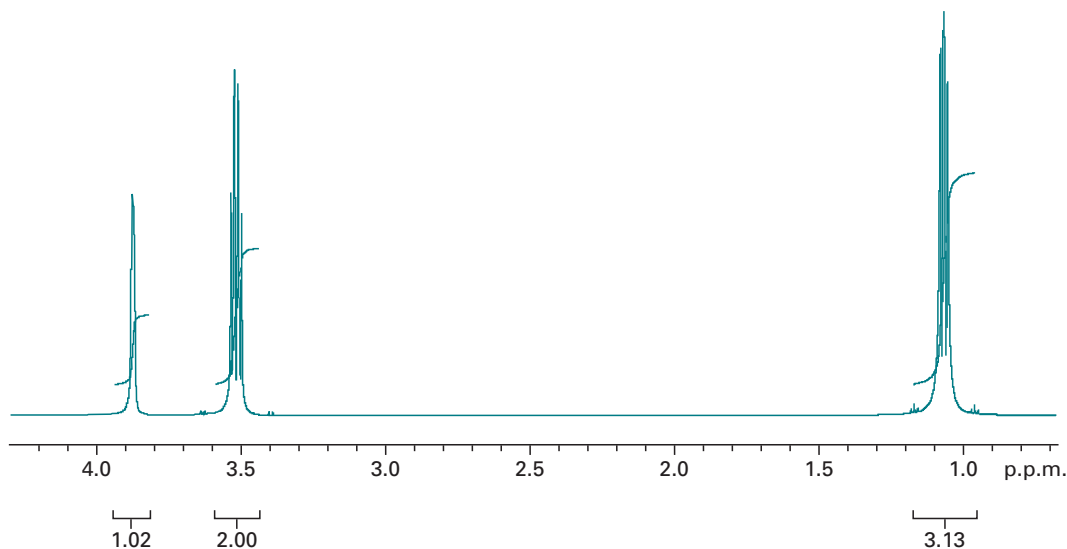


Fig. 13.8  $^1\text{H}$  NMR spectrum of ethyl alcohol ( $\text{H}_3\text{C}-\text{CH}_2-\text{OH}$ ) with integrated peaks.

is proportional to the number of protons of that particular type. Figure 13.8 shows an  $^1\text{H}$  NMR spectrum of ethyl alcohol, in which there are three methyl, two methylene and one alcohol group protons. The peak areas are integrated, and show the proportions 3 : 2 : 1. Owing to the interaction of bonding electrons with like or different spins, a phenomenon called **spin-spin coupling** (also termed **scalar** or **J-coupling**) arises that can extend to nuclei four or five bonds apart. This results in the splitting of the three bands in Fig. 13.8 into several finer bands (hyperfine splitting). The hyperfine splitting yields valuable information about the near-neighbour environment of a nucleus.

NMR spectra are of great value in elucidating chemical structures. Both qualitative and quantitative information may be obtained. The advances in computing power have made possible many more advanced NMR techniques. Weak signals can be enhanced by running many scans and accumulating the data. Baseline noise, which is random, tends to cancel out whereas the signal increases. This approach is known as computer averaging of transients or CAT scanning, and significantly improves the signal-to-noise ratio.

Despite the value and continued use of such 'conventional'  $^1\text{H}$  NMR, much more structural information can be obtained by resorting to pulsed input of radio frequency energy, and subjecting the output to Fourier transform. This approach has given rise to a wide variety of procedures using multidimensional spectra,  $^{13}\text{C}$  and other odd-isotope NMR spectra and the determination of multiplicities and scan images.

#### Pulse-acquire and Fourier transform methods

In 'conventional' NMR spectroscopy, the electromagnetic radiation (energy) is supplied from the source as a continuously changing frequency over a preselected spectral range (continuous wave method). The change is smooth and regular between fixed limits. Figure 13.9a illustrates this approach. During the scan, radiation of

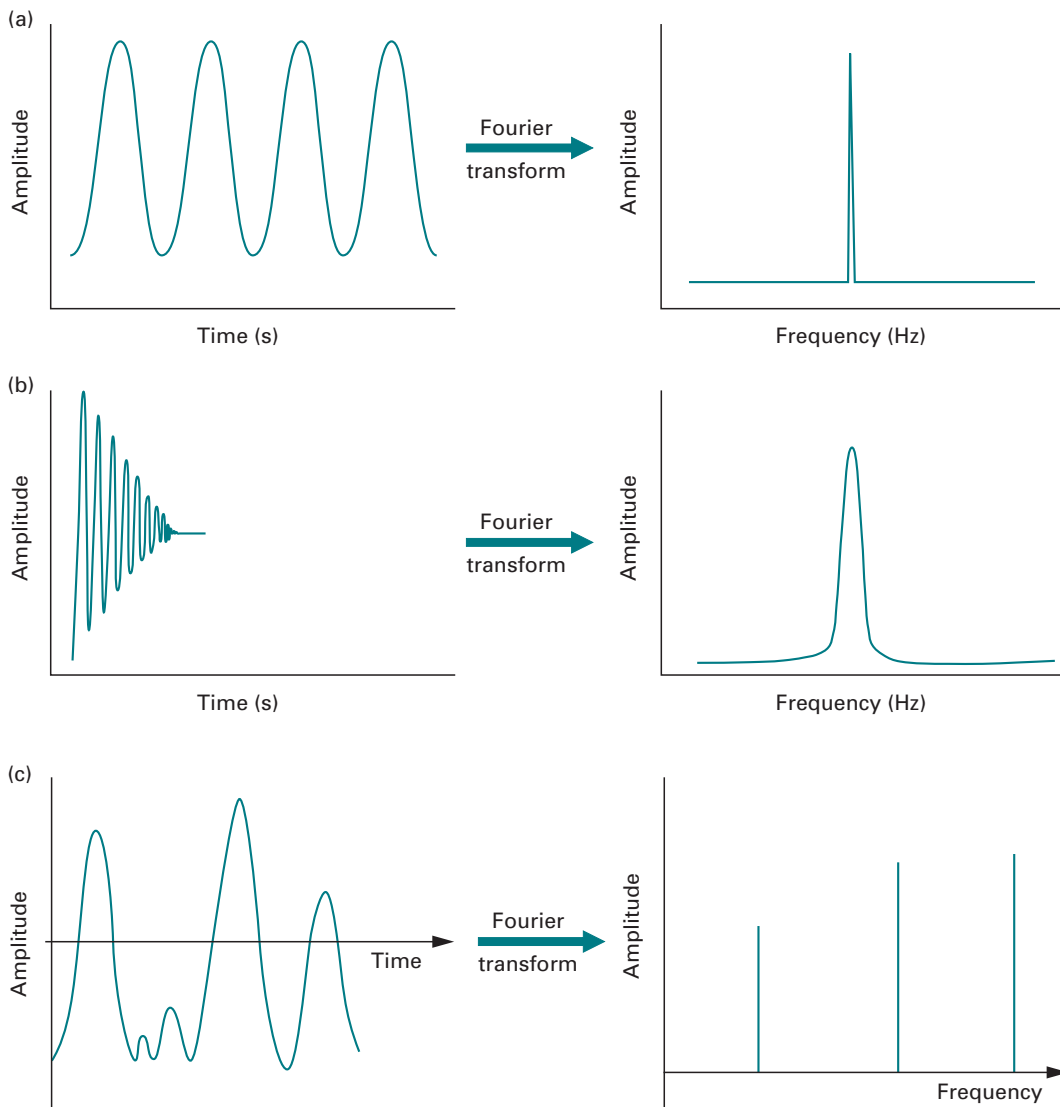


Fig. 13.9 Diagrammatic representation of the Fourier transformation of (a) a single frequency sine wave, (b) a single frequency FID, and (c) a three-sine-wave combination.

certain energy in the form of a sine wave is recorded. By using the mathematical procedure of **Fourier transform**, the 'time domain' can be resolved into a 'frequency domain'. For a single-frequency sine wave, this procedure yields a single peak of fixed amplitude. However, because the measured signal in NMR is the re-emission of energy as the nuclei return from their high-energy into their low-energy states, the recorded radiation will decay with time, as fewer and fewer nuclei will return to the ground state. The signal measured is thus called the **free induction decay** (FID). Figure 13.9b shows the effect of the FID on the corresponding Fourier transform. The frequency band broadens, but the peak position and the amplitude remain the same. The resolved frequency peak represents the chemical shift of a nucleus resonating at this energy.

Alternatively, the total energy comprising all frequencies between the fixed limits can be put in all at the same time. This is achieved by irradiating the sample with a broadband pulse of all frequencies at one go. The output will measure all resonance energies simultaneously and will result in a very complicated interference pattern. However, Fourier transform is able to resolve this pattern into the constituting frequencies (Fig. 13.9c).

In the presence of an external magnetic field, nuclear spins precess around the axis of that field with the so-called **Larmor frequency**. The vector sum of all nuclear magnetic moments yields a magnetisation parallel to the external field, i.e. a **longitudinal magnetisation**. When a high-frequency pulse is applied, the overall magnetisation is forced further off the precession by a pulse angle. This introduces a new vector component to the overall magnetisation which is perpendicular to the external field; this component is called **transverse magnetisation**. The FID measured in pulse-acquired spectra is, in fact, the decay of that transverse magnetisation component.

### Nuclear Overhauser effect

It has already been mentioned above that nuclear spins generate magnetic fields which can exert effects through space, for example as observed in spin-spin coupling. This coupling is mediated through chemical bonds connecting the two coupling spins. However, magnetic nuclear spins can also exert effects in their proximal neighbourhood via dipolar interactions. The effects encountered in the dipolar interaction are transmitted through space over a limited distance on the order of 0.5 nm or less. These interactions can lead to the **nuclear Overhauser effects** (NOEs), as observed in a changing signal intensity of a resonance when the state of a near neighbour is perturbed from the equilibrium. Because of the spatial constraint, this information enables conclusions to be drawn about the three-dimensional geometry of the molecule being examined.

### $^{13}\text{C}$ NMR

Due to the low abundance of the  $^{13}\text{C}$  isotope, the chance of finding two such species next to each other in a molecule is very small (see Chapter 9). As a consequence,  $^{13}\text{C}$ - $^{13}\text{C}$  couplings (homonuclear couplings) do not arise. While  $^1\text{H}$ - $^{13}\text{C}$  interactions (heteronuclear coupling) are possible, one usually records decoupled  $^{13}\text{C}$  spectra where all bands represent carbon only.  $^{13}\text{C}$  spectra are thus much simpler and cleaner when compared to  $^1\text{H}$  spectra. The main disadvantage though is the fact that multiplicities in these spectra cannot be observed, i.e. it cannot be decided whether a particular  $^{13}\text{C}$  is associated with a methyl ( $\text{H}_3\text{C}$ ), a methylene ( $\text{H}_2\text{C}$ ) or a methyne (HC) group. Some of this information can be regained by irradiating with an off-resonance frequency during a decoupling experiment. Another routinely used method is called **distortionless enhancement by polarisation transfer** (DEPT), where sequences of multiple pulses are used to excite nuclear spins at different angles, usually  $45^\circ$ ,  $90^\circ$  or  $135^\circ$ . Although interactions have been decoupled, in this situation the resonances exhibit positive or negative signal intensities dependent on the number of protons bonded to the carbon. In DEPT-135, for example, a methylene group yields a negative intensity, while methyl and methyne groups yield positive signals.

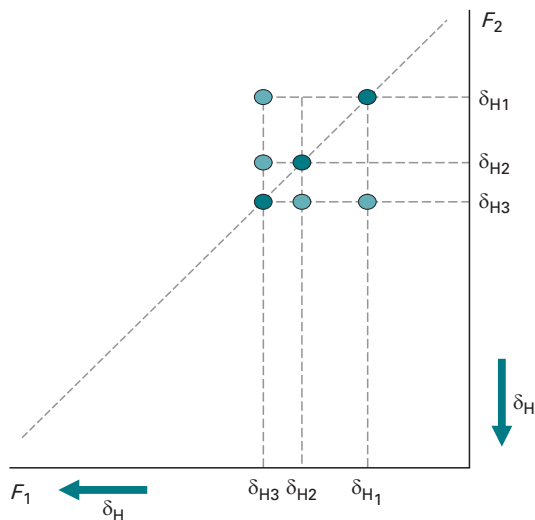


Fig. 13.10 Schematics of a correlated 2D- $^1\text{H}$  NMR spectrum. H3 couples with H2 and H1. H1 and H2 show no coupling.

### Multidimensional NMR

As we learned above, the observable in pulse-acquired Fourier transform NMR is the decay of the transverse magnetisation, called **free induction decay** (FID). The detected signal thus is a function of the detection time  $t_2$ . Within the pulse sequence, the time  $t_1$  (evolution time) describes the time between the first pulse and signal detection. If  $t_1$  is systematically varied, the detected signal becomes a function of both  $t_1$  and  $t_2$ , and its Fourier transform comprises two frequency components. The two components form the basis of a two-dimensional spectrum.

Correlated 2D-NMR spectra show chemical shifts on both axes. Utilising different pulse sequences leads to different methods, such as correlated spectroscopy (COSY), nuclear overhauser effect spectroscopy (NOESY), etc. Such methods yield the homonuclear  $^1\text{H}$  couplings. The 1D-NMR spectrum now appears along the diagonal and long-range couplings between particular nuclei appear as off-diagonal signals (Fig. 13.10).

### Summary of NMR parameters

The parameters obtained from NMR spectra used to derive structural determinants of a small molecule or protein are summarised in Table 13.1.

## 13.5.2 Instrumentation

Schematically, an analytical NMR instrument is very similar to an EPR instrument, except that instead of a klystron generating microwaves two sets of coils are used to generate and detect radio frequencies (Fig. 13.11). Samples in solution are contained in sealed tubes which are rotated rapidly in the cavity to eliminate irregularities and imperfections in sample distribution. In this way, an average and uniform signal

Table 13.1 **NMR-derived structural parameters of molecules**

Parameter	Information	Example/Comment
Chemical shift	Chemical group	$^1\text{H}$ , $^{13}\text{C}$ , $^{15}\text{N}$ , $^{31}\text{P}$
	Secondary structure	
J-couplings (through bond)	Dihedral angles	$^3J(\text{amide-H}, \text{H}\alpha)$ , $^3J(\text{H}\alpha, \text{H}\beta)$ , . . .
NOE (through space)	Interatomic distances	$<0.5 \text{ nm}$
Solvent exchange	Hydrogen bonds	Hydrogen-bonded amide protons are protected from H/D exchange, while the signals of other amides disappear quickly
Relaxation/line widths	Mobility, dynamics, conformational/chemical exchange	The exchange between two conformations, but also chemical exchange, gives rise to two distinct signals for a particular spin
	Torsion angles	
Residual dipolar coupling	Torsion angles	$^1\text{H}-^{15}\text{N}$ , $^1\text{H}-^{13}\text{C}$ , $^{13}\text{C}-^{13}\text{C}$ , . . .

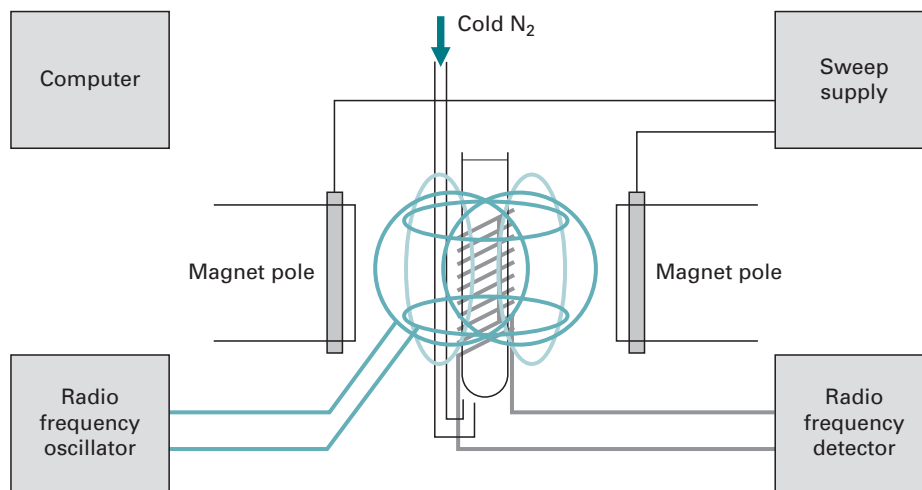


Fig. 13.11 Schematic diagram of an NMR spectrometer with cryoprobe.

is reflected to the receiver to be processed and recorded. In solid samples, the number of spin-spin interactions is greatly enhanced due to intermolecular interactions that are absent in dissolved samples due to translation and rotation movements. As a result, the resonance signals broaden significantly. However, high-resolution spectra can be obtained by spinning the solid sample at an angle of  $54.7^\circ$  (**magic angle spinning**). The sophisticated pulse sequences necessary for multidimensional NMR require

a certain geometric layout of the radio frequency coils and sophisticated electronics. Advanced computer facilities are needed for operation of NMR instruments, as well as analysis of the acquired spectra.

### 13.5.3 Applications

#### Molecular structure determination

Traditionally, NMR spectroscopy is the main method of structure determination for organic compounds. The chemical shift provides a clue about the environment of a particular proton or carbon, and thus allows conclusions as to the nature of functional groups. Spin-spin interactions allow conclusions as to how protons are linked with the carbon skeleton. For structure determination, the fine structure usually is the most useful information because it provides a unique criterion while chemical shifts of some groups can vary over an extended range. Additionally, the signal intensity provides information as to how many protons contribute to a particular signal.

#### Solution structure of proteins and peptides

The structures of proteins up to a mass of about 50 kDa can be determined with biomolecular NMR spectroscopy. The development of magnets with very high field strengths (currently 900 MHz) continues to push the size limit. The preparation of proteins or selected domains for NMR requires recombinant expression and isotopic labelling to enrich the samples with  $^{13}\text{C}$  and  $^{15}\text{N}$ ;  $^2\text{H}$  labelling might be required as well. Sample amounts in the order of 10 mg used to be required for NMR experiments; however, the introduction of cryoprobe technology has reduced the sample amount significantly. Heteronuclear multidimensional NMR spectra need to be recorded for the assignment of all chemical shifts ( $^1\text{H}$ ,  $^{13}\text{C}$ ,  $^{15}\text{N}$ ). For interproton NOEs,  $^{13}\text{C}$ - and  $^{15}\text{N}$ -edited 3D NOESY spectra are required. The data acquisition can take several weeks, after which spectra are processed (Fourier transformation) and improved with respect to digital resolution and signal-to-noise. Assignment of chemical shifts and interatomic distances is carried out with the help of software programs. All experimentally derived parameters are then used as restraints in a molecular dynamics or simulated annealing structure calculation. The result of a protein NMR structure is an ensemble of structures, all of which are consistent with the experimentally determined restraints, but converge to the same fold.

#### Magnetic resonance imaging

The basic principles of NMR can be applied to imaging of live samples. Because the proton is one of the more sensitive nuclides and is present in all biological systems abundantly,  $^1\text{H}$  resonance is used almost exclusively in the clinical environment. The most important compound in biological samples in this context is water. It is distributed differently in different tissues, but constitutes about 55% of body mass in the average human. In soft tissues, the water distribution varies between 60% and 90%. In NMR, the resonance frequency of a particular nuclide is proportional to the

**Example 2 ASSESSING PROTEIN CONFORMATIONAL EXCHANGE BY NMR**

**Question** Identification of protein–protein interaction sites is crucial for understanding the basis of molecular recognition. How can such sites be identified?

**Answer** Apart from providing the absolute three-dimensional structure of molecules, NMR methods can also yield insights into protein interactions by mapping. In a technique called saturation transfer difference NMR, protein resonances can be selectively saturated. One then calculates the  $^1\text{H}$  NMR difference spectrum of the ligand from the saturation experiment subtracted from the ligand spectrum without saturation of the protein. Intensities of protons in close contact with the ligand appear enhanced in the difference spectrum, allowing the identification of chemical groups of the ligand interacting with the protein. Using titration experiments, this technique also allows determination of binding constants.

Beyond mapping the flexibility of residues in known protein binding sites, NMR techniques can also be used to identify novel binding sites in proteins. Protein motions on the timescale of microseconds to milliseconds are accessible to NMR spectroscopy, and the diffusion constants for rotation around the three principal axes  $x$ ,  $y$  and  $z$  (called rotational diffusion tensor) can be determined. The principal axes are fixed in the protein, and the principal components as well as the orientation can be derived from analysis of the ratio of the spin–spin and spin–lattice relaxation times  $T_2/T_1$ . Analysing these values for the protons of the rigid amide (CO–NH) groups allows a characterisation of the conformational exchange of proteins.

Residues constituting the ligand–binding interface often experience a different environment in the bound state as compared to the free state. The amide signals of these residues are thus broadened due to exchange between these two environments when the free and bound states are in equilibrium.

This approach has been successfully applied to identify the amino acids at the binding site of a 16 kDa protein that binds to and regulates the 251 kDa hydroxylase of the methane monooxygenase protein system. The free and bound forms of the regulatory protein exchange on the timescale of milliseconds.

Other examples include the identification of specific sites involved in the weak self-association of the N-terminal domain of the rat T-cell adhesion protein CD2 (CD2d1) using the concentration dependence of the  $T_2$  values.

strength of the applied external magnetic field. If an external magnetic field gradient is applied then a range of resonant frequencies are observed, reflecting the spatial distribution of the spinning nuclei. **Magnetic resonance imaging** (MRI) can be applied to large volumes in whole living organisms and has a central role in routine clinical imaging of large-volume soft tissues.

The number of spins in a particular defined spatial region gives rise to the spin density as an observable parameter. This measure can be combined with analysis of



Fig. 13.12 Magnetic resonance imaging: 2-mm thick coronal  $T_2$  weighted fast spin echo image at the level of the foramina monroi connecting the anterior horns of the lateral ventricles with the third ventricle. The sequence consisting of 40 images was acquired at a field strength of 3 tesla and generates  $0.47 \times 0.64 \times 2$  mm voxels. (Image courtesy of Professor H. Urbach, University of Bonn.)

the principal relaxation times ( $T_1$  and  $T_2$ ). The imaging of flux, as either bulk flow or localised diffusion, adds considerably to the options available. In terms of whole-body scanners, the entire picture is reconstructed from images generated in contiguous slices. MRI can be applied to the whole body or specific organ investigations on head, thorax, abdomen, liver, pancreas, kidney and musculoskeletal regions (Fig. 13.12). The use of contrast agents with paramagnetic properties has enabled investigation of organ function, as well as blood flow, tissue perfusion, transport across the blood-brain barrier and vascular anatomy. Resolution and image contrast are major considerations for the technique and subject to continuing development. The resolution depends on the strength of the magnetic field and the availability of labels that yield high signal strengths. MRI instruments used for clinical imaging typically operate with field strengths of up to 3 T, but experimental instruments can operate at more than 20 T, allowing the imaging of whole live organisms with almost enough spatial and temporal resolution to follow regenerative processes continuously at the single-cell level. Equipment cost and data acquisition time remain important issues. On the other hand, according to current knowledge, MRI has no adverse effects on human health, and thus provides a valuable diagnostic tool, especially due to the absence of the hazards of ionising radiation.



## 13.6 X-RAY DIFFRACTION

### 13.6.1 Principles

The interaction of electromagnetic radiation with matter causes the electrons in the exposed sample to oscillate. The accelerated electrons, in turn, will emit radiation of the same frequency as the incident radiation, called the secondary waves. The superposition of waves gives rise to the phenomenon of **interference**. Depending on the displacement (phase difference) between two waves, their amplitudes either reinforce or cancel each other out. The maximum reinforcement is called **constructive interference**, the cancelling is called **destructive interference**. The interference gives rise to dark and bright rings, lines or spots, depending on the geometry of the object causing the diffraction. Diffraction effects increase as the physical dimension of the diffracting object (aperture) approaches the wavelength of the radiation. When the aperture has a periodic structure, for example in a diffraction grating, repetitive layers or crystal lattices, the features generally become sharper. **Bragg's law** (Fig. 13.13) describes the condition that waves of a certain wavelength will constructively interfere upon partial reflection between surfaces that produce a path difference only when that path difference is equal to an integral number of wavelengths. From the constructive interferences, i.e. diffraction spots or rings, one can determine dimensions in solid materials.

Since the distances between atoms or ions are on the order of  $10^{-10}$  m (1 Å), diffraction methods used to determine structures at the atomic level require radiation in the X-ray region of the electromagnetic spectrum, or beams of electrons or neutrons with a similar wavelength. While electrons and neutrons are particles, they also possess wave properties with the wavelength depending on their energy (**de Broglie hypothesis**). Accordingly, diffraction can also be observed using electron and neutron beams. However, each method also has distinct features, including the penetration depth which increases in the series electrons – X-rays – neutrons.

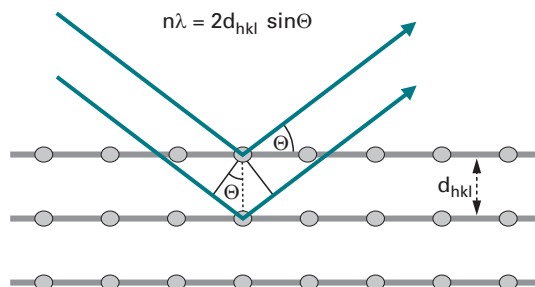


Fig. 13.13 Bragg's law. Interference effects are observable only when radiation interacts with physical dimensions that are approximately the same size as the wavelength of the radiation. Only diffracted beams that satisfy the Bragg condition are observable (constructive interference). Diffraction can thus be treated as selective reflection.  $n$  is an integer ('order'),  $\lambda$  is the wavelength of the radiation,  $d$  is the spacing between the lattice planes and  $\Theta$  is the angle between the incident/reflected beam and the lattice plane.

### 13.6.2 X-ray diffraction

X-rays for chemical analysis are commonly obtained by **rotating anode generators** (in-house) or **synchrotron** facilities (Fig. 13.14). In rotating anode generators, a rotating metal target is bombarded with high-energy (10–100 keV) electrons that knock out core electrons. An electron in an outer shell fills the hole in the inner shell and emits the energy difference between the two states as an X-ray photon. Common targets are copper, molybdenum and chromium, which have strong distinct X-ray emission at 1.54 Å, 0.71 Å and 2.29 Å, respectively, that is superimposed on a continuous spectrum known as **Bremsstrahlung**. In synchrotrons, electrons are accelerated in a ring, thus producing a continuous spectrum of X-rays. Monochromators are required to select a single wavelength.

As X-rays are diffracted by electrons, the analysis of X-ray diffraction data sets produces an **electron density** map of the crystal. Since hydrogen atoms have very little electron density, they are not usually determined experimentally by this technique.

Unfortunately, the detection of light beams is restricted to recording the intensity of the beam only. Other properties, such as polarisation, can only be determined with rather complex measurements. The phase of the light waves is even systematically lost in the measurement. This phenomenon has thus been termed the **phase problem**.

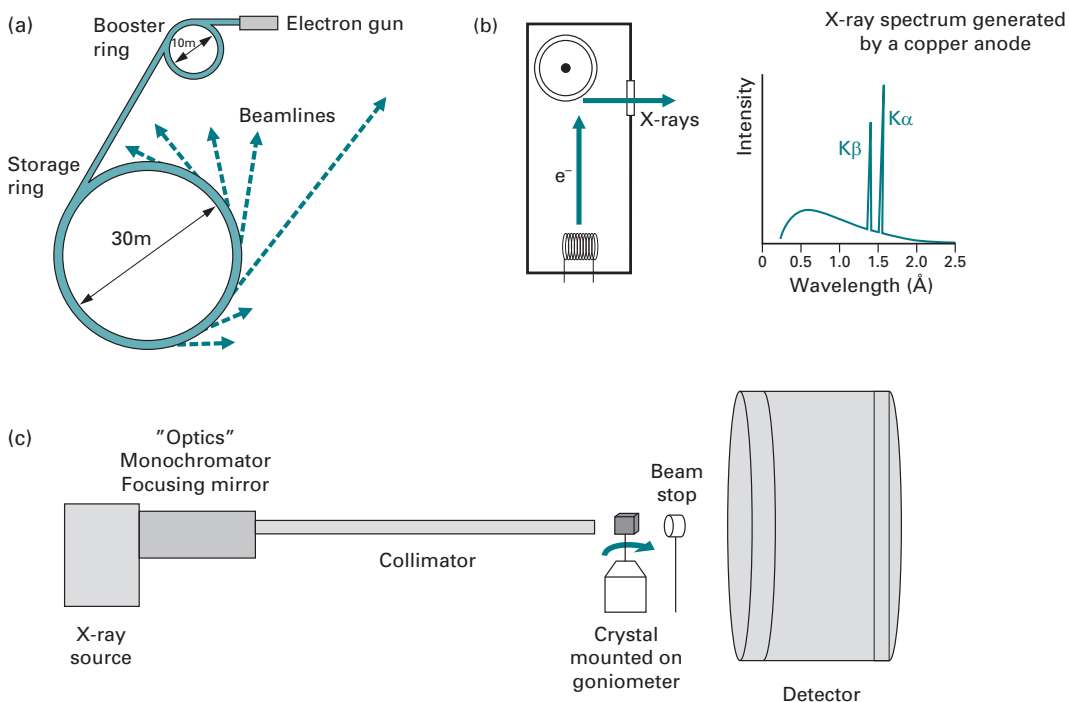


Fig. 13.14 Instrumentation for X-ray diffraction. The most common X-ray sources are (a) particle storage rings which produce synchrotron radiation, and (b) rotating anode tubes. The schematics of an X-ray diffractometer are shown in (c).

owing to the essential information contained in the phase in diffraction and microscopy experiments. The X-ray diffraction data can be used to calculate the amplitudes of the three-dimensional Fourier transform of the electron density. Only together with the phases can the electron density be calculated, in a process called Fourier synthesis.

Different methods to overcome the phase problem in X-ray crystallography have been developed, including:

- molecular replacement, where phases from a structurally similar molecule are used;
- experimental methods that require incorporation of heavy element salts (multiple isomorphous replacement);
- experimental methods where methionine has been replaced by seleno-methionine in proteins (multi-wavelength anomalous diffraction);
- experimental methods using the anomalous diffraction of the intrinsic sulphur in proteins (single wavelength anomalous diffraction);
- direct methods, where a statistical approach is used to determine phases. This approach is limited to very high resolution data sets and is the main method for small molecule crystals as these provide high-quality diffraction with relatively few numbers of reflections.

### 13.6.3 Applications

#### Single-crystal diffraction

A crystal is a solid in which atoms or molecules are packed in a particular arrangement within the **unit cell** which is repeated indefinitely along three principal directions in space. Crystals can be formed by a wide variety of materials, such as salts, metals, minerals and semiconductors, as well as various inorganic, organic and biological molecules.

A crystal grown in the laboratory is mounted on a goniometer and exposed to X-rays produced by rotating anode generators (in-house) or a synchrotron facility. A diffraction pattern of regularly spaced spots known as reflections is recorded on a detector, most frequently image plates or CCD cameras for proteins, and moveable proportional counters for small molecules.

An incident X-ray beam is diffracted by a crystal such that beams at specific angles are produced, depending on the X-ray wavelength, the crystal orientation and the structure of the crystal (i.e. unit cell).

To record a data set, the crystal is gradually rotated and a diffraction pattern is acquired for each distinct orientation. These two-dimensional images are then analysed by identifying the appropriate reflection for each **lattice plane** and measuring its intensity, measuring the cell parameters of the unit cell and determining the appropriate space group. If information about the phases is available, this data can then be used to calculate a three-dimensional model of the electron density within the unit cell using the mathematical method of Fourier synthesis. The positions of the atomic nuclei are then deduced from the electron density by computational refinement and manual intervention using molecular graphics.

### Fibre diffraction

Certain biological macromolecules, such as DNA and cytoskeletal components, cannot be crystallised, but form fibres. In fibres, the axes of the long polymeric structures are parallel to each other. While this can be an intrinsic property, for example in muscle fibres, in some cases the parallel alignment needs to be induced. As fibres show **helical symmetry**, by analysing the diffraction from oriented fibres one can deduce the helical symmetry of the molecule, and in favourable cases the molecular structure. Generally, a model of the fibre is constructed and the expected diffraction pattern is compared with the observed diffraction.

Historically, fibre diffraction was of central significance in enabling the determination of the three-dimensional structure of DNA by Crick, Franklin, Watson and Wilkins.

Two classes of fibre diffraction patterns can be distinguished. In **crystalline fibres** (e.g. A form of DNA), the long fibrous molecules pack to form thin micro-crystals randomly arranged around a shared common axis. The resulting diffraction pattern is equivalent to taking a long crystal and spinning it about its axis during the X-ray exposure. All Bragg reflections are recorded at once. In **non-crystalline fibres** (e.g. B form of DNA), the molecules are arranged parallel to each other but in a random orientation around the common axis. The reflections in the diffraction pattern are now a result of the periodic repeat of the fibrous molecule. The diffraction intensity can be calculated via Fourier–Bessel transformation replacing the Fourier transformation used in single-crystal diffraction.

### Powder diffraction

Powder diffraction is a rapid method to analyse multicomponent mixtures without the need for extensive sample preparation. Instead of using single crystals, the solid material is analysed in the form of a powder where, ideally, all possible crystalline orientations are equally represented.

From powder diffraction patterns, the interplanar spacings  $d$  of the lattice planes (Fig. 13.13) are determined and then compared to a known standard or to a database (Powder Diffraction File by the International Centre for Diffraction Data or the Cambridge Structural Database) for identification of the individual components.

## 13.7 SMALL-ANGLE SCATTERING

The characteristics of molecules at larger size scales are fundamentally different than at atomic scales. While atomic scale structures are characterised by high degrees of order (e.g. crystals), on the nano scale, the building blocks of matter are rarely well organised and are composed of rather complex building blocks (i.e. shapes). Consequently, sharp diffraction peaks are observed in X-ray diffraction from single crystals, but diffuse patterns are obtained from X-ray scattering from biological molecules or nano-structures.

In Section 12.6, we learned that incident light scattered by a particle in the form of **Rayleigh scattering** has the same frequency as the incident light. It is thus called elastic light scattering. The light scattering techniques discussed in Section 12.6 have used a

combination of visible light and molecules, so that the dimension of the particle is smaller than the wavelength of the light. When using light of smaller wavelengths such as X-rays, the overall dimension of a molecule is large as compared to the incident light. Electrons in the different parts of the molecule are now excited by the incident beam with different phases. The coherent waves of the scattered light therefore show an interference that is dependent on the geometrical shape of the molecule. As a result

- in the forward direction (at  $0^\circ$ ), there is no phase difference between the waves of the scattered light, and one observes maximum positive interference, i.e. highest scattering intensity;
- at small angles, there is a small but significant phase difference between the scattered waves which results in diminished scattering intensity due to destructive interference.

**Small-angle X-ray** or **neutron scattering** (SAXS or SANS) are experimental techniques used to derive size and shape parameters of large molecules. Both X-ray and neutron scattering are based on the same physical phenomenon, i.e. scattering due to differences in scattering mass density between the solute and the solvent or indeed between different molecular constituents. An advantage for protein structure determination is the fact that samples in aqueous solution can be assessed.

Experimentally, a monodisperse solution of macromolecules is exposed to either X-rays (wavelength  $\lambda = \text{ca. } 0.15 \text{ nm}$ ) or thermal neutrons ( $\lambda = \text{ca. } 0.5 \text{ nm}$ ). The intensity of the scattered light is recorded as a function of momentum transfer  $q$  ( $q = 4\pi \sin \theta \lambda^{-1}$ , where  $2\theta$  is the angle between the incident and scattered radiation). Due to the random positions and orientations of particles, an isotropic intensity distribution is observed that is proportional to the scattering from a single particle averaged over all orientations. In neutron scattering, the **contrast** (squared difference in scattering length density between particle and solvent) can be varied using  $\text{H}_2\text{O}/\text{D}_2\text{O}$  mixtures or selective deuteration to yield additional information. At small angles the scattering curve is a rapidly decaying function of  $q$ , and essentially determined by the **particle shape**. Fourier transformation of the scattering function yields the so-called **size distribution function** which is a histogram of interatomic distances. Comparison of the size distribution function with the particle form factor of regular geometrical bodies allows conclusions as to the shape of the scattering particle. Analysis of the scattering function further allows determination of the **radius of gyration**  $R_g$  (average distance of the atoms from the centre of gravity of the molecule), and the mass of the scattering particle from the scattering in the forward direction.

### Shape restoration

Software programs have been developed that enable the calculation of three-dimensional structures from the one-dimensional scattering data obtained by SAXS. Due to the low resolution of SAXS data, the structural information is restricted to the shape of the scattering molecules. Furthermore, the scattering data do not imply a single, unique solution. The reconstruction of three-dimensional structures might thus result in a number of different models. One approach is to align and average a set of independently reconstructed models thus obtaining a model that retains the most persistent features.

## 13.8 SUGGESTIONS FOR FURTHER READING

**General**

Ciulli, A. and Abell, C. (2007). Fragment-based approaches to enzyme inhibition. *Current Opinion in Biotechnology*, 18, 489–496.

**Infrared spectroscopy**

Beekes, M., Lasch, P. and Naumann, D. (2007). Analytical applications of Fourier transform-infrared (FT-IR) spectroscopy in microbiology and prion research. *Veterinary Microbiology*, 123, 305–319.

Ganim, Z., Chung, H. S., Smith, A. W., Deflores, L. P., Jones, K. C. and Tokmakoff, A. (2008). Amide I two-dimensional infrared spectroscopy of proteins. *Accounts of Chemical Research*, 41, 432–441.

Tonouchi, M. (2007). Cutting-edge terahertz technology. *Nature Photonics*, 1, 97–105.

**WEBSITES**

<http://www.cem.msu.edu/~reusch/VirtualText/Spectrpy/InfraRed/infrared.htm>

<http://www.chem.uic.edu/web1/ocol/spec/IR.htm>

<http://orgchem.colorado.edu/hndbksupport/irtutor/tutorial.html>

<http://www.umd.umich.edu/casl/natsci/slc/slconline/IR/>

<http://www.biophysik.uni-freiburg.de/Spectroscopy/Time-Resolved/spectroscopy.html>

**Raman spectroscopy**

Benevides, J. M., Overman, S. A. and Thomas, G. J. Jr. (2004). Raman spectroscopy of proteins.

*Current Protocols in Protein Science*, Chapter 17, Unit 17.8. New York: Wiley Interscience.

Wen, Z. Q. (2007). Raman spectroscopy of protein pharmaceuticals. *Journal of Pharmaceutical Sciences*, 96, 2861–2878.

**WEBSITES**

<http://www.jobinyvon.com/Raman%20Tutorial%20Intro>

<http://people.bath.ac.uk/pysdw/newpage11.htm>

**Surface plasmon resonance**

Anker, J. N., Hall, W. P., Lyandres, O., Shah, N. C., Zhao, J. and Van Duyne, R. P. (2008). Biosensing with plasmonic nanosensors. *Nature Materials*, 7, 442–453.

Campbell, C. T. and Kim, G. (2007). SPR microscopy and its applications to high-throughput analyses of biomolecular binding events and their kinetics. *Biomaterials*, 28, 2380–2392.

Majka, J. and Speck, C. (2007). Analysis of protein–DNA interactions using surface plasmon resonance. *Advances in Biochemical Engineering and Biotechnology*, 104, 13–36.

Neumann, T., Junker, H. D., Schmidt, K. and Sekul, R. (2007). SPR-based fragment screening: advantages and applications. *Current Topics in Medicinal Chemistry*, 7, 1630–1642.

Phillips, K. S. and Cheng, Q. (2007). Recent advances in surface plasmon resonance based techniques for bioanalysis. *Analytical and Bioanalytical Chemistry*, 387, 1831–1840.

**WEBSITES**

<http://www.biacore.com/>

<http://www.uksaf.org/tech/spr.html>

<http://people.clarkson.edu/~ekatz/spr.htm>

**Electron paramagnetic resonance spectroscopy**

Matsumoto, K., Subramanian, S., Murugesan, R., Mitchell, J. B. and Krishna, M. C. (2007). Spatially resolved biologic information from in vivo EPRI, OMRI, and MRI. *Antioxidants and Redox Signaling*, 9, 1125–1141.

Schiemann, O. and Prisner, T. F. (2007). Long-range distance determinations in biomacromolecules by EPR spectroscopy. *Quarterly Reviews in Biophysics*, 40, 1–53.

**WEBSITES**

<http://hyperphysics.phy-astr.gsu.edu/hbase/molecule/esr.html>

<http://www.chemistry.nmsu.edu/studntres/chem435/Lab7/intro.html>

**Nuclear magnetic resonance spectroscopy**

- Blamire, A. M. (2008). The technology of MRI: the next 10 years? *British Journal of Radiology*, **81**, 601–617.
- Ishima, R. and Torchia, D. A. (2000). Protein dynamics from NMR. *Nature Structural Biology*, **7**, 740–743.
- McDermott, A. and Polenova, T. (2007). Solid state NMR: new tools for insight into enzyme function. *Current Opinion in Structural Biology*, **17**, 617–622.
- Skinner, A. L. and Laurence, J. S. (2008). High-field solution NMR spectroscopy as a tool for assessing protein interactions with small molecule ligands. *Journal of Pharmaceutical Science*, **97**, 4670–4695.
- Spiess, H. W. (2008). NMR spectroscopy: pushing the limits of sensitivity. *Angewandte Chemie International Edition (English)*, **47**, 639–642.

**WEBSITES**

- <http://www.cem.msu.edu/~reusch/VirtualText/Spectrpy/nmr/nmr1.htm#nmr1>
- [http://arrhenius.rider.edu/nmr/NMR\\_tutor/pages/nmr\\_tutor\\_home.html](http://arrhenius.rider.edu/nmr/NMR_tutor/pages/nmr_tutor_home.html)
- <http://www.cis.rit.edu/htbooks/nmr/>
- <http://teaching.shu.ac.uk/hwb/chemistry/tutorials/molspec/nmr1.htm>
- <http://www.chem.queensu.ca/FACILITIES/NMR/nmr/webcourse/>

**X-ray diffraction**

- Hickman, A. B. and Davies, D. R. (2001). Principles of macromolecular X-ray crystallography. *Current Protocols in Protein Science*, Chapter 17, Unit 17.3. New York: Wiley Interscience.
- Miao, J., Ishikawa, T., Shen, Q. and Earnest, T. (2008). Extending X-ray crystallography to allow the imaging of noncrystalline materials, cells, and single protein complexes. *Annual Reviews in Physical Chemistry*, **59**, 387–410.
- Mueller, M., Jenni, S. and Ban, N. (2007). Strategies for crystallization and structure determination of very large macromolecular assemblies. *Current Opinion in Structural Biology*, **17**, 572–579.
- Wlodawer, A., Minor, W., Dauter, Z. and Jaskolski, M. (2008). Protein crystallography for non-crystallographers, or how to get the best (but not more) from published macromolecular structures. *FEBS Journal*, **275**, 1–21.

**WEBSITES**

- <http://www.colorado.edu/physics/2000/xray/index.html>
- <http://www.physics.upenn.edu/~heiney/talks/hires/hires.html>
- <http://www.matter.org.uk/diffraction/x-ray/default.htm>

**Small-angle scattering**

- Lipfert, J. and Doniach, S. (2007). Small-angle X-ray scattering from RNA, proteins, and protein complexes. *Annual Reviews of Biophysical and Biomolecular Structure*, **36**, 307–327.
- Neylon, C. (2008). Small angle neutron and X-ray scattering in structural biology: recent examples from the literature. *European Biophysics Journal*, **37**, 531–541.
- Putnam, C. D., Hammel, M., Hura, G. L. and Tainer, J. A. (2007). X-ray solution scattering (SAXS) combined with crystallography and computation: defining accurate macromolecular structures, conformations and assemblies in solution. *Quarterly Reviews in Biophysics*, **40**, 191–285.

**WEBSITES**

- <http://www.ncnr.nist.gov/programs/sans/tutorials/index.html>
- <http://www.isis.rl.ac.uk/largescale/loq/documents/sans.htm>
- <http://www.embl-hamburg.de/workshops/2001/EMBO/>